Title:

AKAP8 interacting with DDX5 to regulate R-loop balance involves in lung carcinoma cell growth

Xu Wang, Dajiang Qin, Liang Liu

Author information:

Xu Wang:
Guangzhou Laboratory, Guangzhou, Guangdong, 510005, China.
wang_xu2@gzlab.ac.cn

Dajiang Qin:
Key Laboratory of Biological Targeting Diagnosis, Therapy and Rehabilitation of Guangdong Higher Education Institutes, The Fifth Affiliated Hospital of Guangzhou Medical University, Guangzhou, Guangdong, 510799, China.
qin_dajiang@gzhmu.edu.cn

Liang Liu:
Guangzhou Laboratory, Guangzhou, Guangdong, 510005, China; State Key Laboratory of Dampness Syndrome of Chinese Medicine, The Second Affiliated Hospital of Guangzhou University of Chinese Medicine, Guangzhou, Guangdong, 510120, China.
liu_liang@gzlab.ac.cn

Corresponding author:

Xu Wang: (+86) 15901025256
Liang Liu: (+86) 15920798553

Abstract

Triple-nucleotide chain of RNA:DNA hybrid structure R-loop is formed during transcription process which is closely associated with transcriptional regulation, transcriptional termination, epigenetic modifications, and structure of chromatin. Dysregulation of R-loop formation or resolution may disturb normal DNA replication or RNA transcription, leading to associated progress of disease. Herein, we found A-kinase-anchoring protein 8 (AKAP8) bind with R-loop structure in cell. Knock down of AKAP8 showed perturbation of balance of genomic R-loop formation and gene transcription. Evidences was shown that AKAP8 interacted with R-loop resolution protein ATP-dependent DEAD box RNA helicase DDX5 and increased chromatin associated DDX5 level. Finally, AKAP8 promoted UCP2 transcription and resolved R-loop level of its promoter region, and contributed to cell growth of adenocarcinomic human alveolar basal epithelial cell line A549, which may provide clues for poor prognosis of lung adenocarcinoma in high AKAP8 expression patients.

Key words: lung carcinoma, AKAP8, R-loop

Introduction

The R-loop is composed of tri-strand nucleic acid structure formed during transcription process. One chain of the double strand DNA is replaced by RNA chain complementary to the other strand DNA chain to form an RNA:DNA hybrid along with a exposed single DNA strand. It is thermodynamically more stable than double strand DNA (Thomas et al. 1976). R-loop is well knowledge as double edged sword for its advantages and disadvantages for cell metabolism. On the one hand, R-loop plays roles in regulation of transcription by multiple mechanism, like participate in promoter methylation, transcription factor binding, or transcription termination (Grunseich et al. 2018) (Chen et al. 2015) (Boque-Sastre et al. 2015). In addition, R-loop is indispensable for replication of bacterial plasmid and human mitochondrial genome (Renaudin et al. 2021). Also, it is necessary for process of animal immunoglobulin gene class switch recombination to generate types of antibody (Refaat et al. 2023).

On the other hand, the disadvantage of R-loop mainly addressed by its destruction to DNA. R-loop makes DNA more sensitive to damages, including transcription dependent DNA recombination, double strand DNA breaks, fragile site instability or even severe chromosome loss (Groh and Gromak 2014). Since R-loop regulates transcription profile of cell, unexpected dysregulation of R-loop by abnormal accumulation or resolution is closely associated with disease in some cases. Mutation of RNA:DNA helicase SETX cause neurodegeneration in adolescent predominant amyotrophic lateral sclerosis type 4 (ALS4) (Kannan et al. 2022). Cell of autoimmune disease Aicardi-Goutieres syndrome (AGS) accumulates R-loop and significantly activates cGAS-STING pathway, which is regarded to associate with RNase H mutation responding for cellular resolution of RNA:DNA (Lim et al. 2015) (Crow and Manel 2015). Mutation driving metabolism perturbation and R-loop accumulation induced DNA damage or blockade of transcriptional complex by breast cancer susceptibility factor BRCA is sort of related to breast tumorigenesis (Tan et al. 2017). In immune cells, unexpected R-loop accumulation simultaneously in immunoglobulin switch gene and its translocation partner including oncogene c-MYC enhance the pathological translocation of them performed by activation induced cytosine deaminase (AID) (Ruiz et al. 2011). Therefore, identification and revelation of R-loop associated protein can provide a basis for elucidation of R-loop regulatory mechanism and diagnostic strategy for disease.

Helicases are kind of family involving in R-loop metabolism. So far, several important helicases including RNA/DNA helicase Senataxin SETX, Auarius AQR, DNA helicase RECO5, RNA helicase DDX1, DDX5, DDX19, DDX21, DHX9 participate in R-loop formation and resolution (Ribeiro de Almeida et al. 2018) (Mersaoui et al. 2019) (Chakraborty et al. 2018). DEAD-box (DDX) protein containing conserved motifs including eponymous DEAD motif (Asp-Glu-Ala-Asp, D-E-A-D) are defined as largest family of double strand RNA helicase (Linder and Jankowsky 2011). DDX5 as coregulator for cellular transcription and splicing, and participator in processing of small noncoding RNA is previously shown to unwind RNA:RNA, RNA:DNA, and R-loop in vitro (Xing et al. 2017) (Mersaoui et al. 2019). Deficiency of DDX5 accumulates R-loop at propensity loci to form such structure in U2OS cell line. It is reported DDX5 is associated with XRN2 exoribonuclease to resolve R-loop resulting in release of RNA

Pol II from transcriptional termination regions (Mersaoui et al. 2019). After, some co-factor of DDX5 involving in its R-loop resolution are claimed including ATPase family AAA domain-containing protein 5 (ATAD5) restricting R-loop formation at replication fork, Yamanaka factor SOX2 inhibiting R-loop resolvase activity of DDX5, thyroid hormone receptor-associated protein 3 (Thrap3), topoisomerase III-beta (TOP3B) and THO complex subunit 5 homolog (THOC5), Treacle ribosome biogenesis factor 1 (TCOF1) promoting R-loop resolution (Kim et al. 2020) (Li et al. 2020b) (Kang et al. 2021) (Saha et al. 2022) (Polenkowski et al. 2023) (Nie et al. 2023). The resolvase activity of DDX5 is also dependent on its post modification. Protein arginine methyltransferase 5 (PRMT5) methylates DDX5 at its RGG/RG motif which promotes DDX5 interaction with XRN2 and repression of cellular R-loops (Mersaoui et al. 2019). Therefore DDX5 and associated proteins cooperate to regulate R-loop formation and resolution during genetic process. The unexpectable aberrant expression of them may impair cellular metabolism and contribute to disease progression. Sox2 interacting with DDX5 inhibits the R-loop resolvase activity of DDX5 to thus facilitate reprogramming (Li et al. 2020b). In Gastric cancer (GC), aberrantly high expression of TCOF1 cooperating with DDX5 contribute to maintaining GC cell proliferation though alleviating R-loop associated DNA replication stress (Nie et al. 2023). Besides of its function in R-loop, DDX5 resolves G4 structure of oncogene MYC promoter to regulate its transcriptional activation (Wu et al. 2019). Positive prognostic factor DDX5 expression is negatively associated with MYC expression in lung cancer (Cui et al. 2021).

In this study, we identified R-loop binding protein A-kinase anchoring protein 8 (AKAP8, also known as AKAP95) was associated with DDX5. AKAP8 is member of AKAP family protein with three classical domain of protein kinase A (PKA) binding domain exerting by hydrophobic face of conserved amphipathic helix, targeting sequence serving to tether the complex to specific subcellular compartment, and signal molecular binding domain elevating second messenger cyclic AMP (cAMP) (Langeberg and Scott 2005). Most of AKAPs reside in the cytoplasm except several members including AKAP8, AKAP8 homologue AKAP8L, and splicing factor SFRS17A (known as AKAP17A) (Kubota et al. 2015) (Martins et al. 2003) (Jarnaess et al. 2009) . For AKAP8, it is reported it regulates nuclear PKA though local cAMP from organized nuclear microdomain consisting of AKAP8, PKA, PDE4D5 (Clister et al. 2019). Besides of its classical kinase anchoring function, AKAP8 capacity of binding with RNA involves in transcription and splicing regulation. AKAP8 and selected partner hnRNPs cooperated to regulate alternative splicing (Hu et al. 2016) (Li et al. 2020a). In vitro and in cell, AKAP8 formed liquid like condensate. The regulatory ability of AKAP8 in transcription and splicing requires its special biophysical property of formed condensate with properly dynamic liquid-liquid phase separation and exchange (Li et al. 2020a). AKAP8 depleted cells shows accelerated EMT and enhanced breast cancer metastatic potential (Hu et al. 2020). The amplification and upregulation of AKAP8 in triple negative breast cancer (TNBC) are found to be correlated with poorer patient survival and its deficiency reduced growth of TNBC cell line (Li et al. 2020a). AKAP8 is determined to interact with connexin 43 (Cx43) in a dynamic pattern during cell cycle progression in lung carcinoma cell line by which regulated cell proliferation (Chen et al. 2016) (Chen et al. 2020). However, the pathophysiologic roles of AKAP8 is so far poorly undertaken.

Herein, we identified AKAP8 was R-loop association protein. Further deciphering interaction between AKAP8 and DDX5, we claimed that AKAP8 slightly enhance chromatin associated DDX5 level and regulated R-loop resolution resulting in transcription changes. It was also suggested this regulation pattern of AKAP8 may contribute to lung carcinoma cell growth offering it as potential prognostic target for lung cancer.

Results

HBD-TurboID for identification of R-loop associated protein. HBD is responding for RNA:DNA hybrid recognize from RNase H N terminal domain. TurboID were recombined expression with HBD and nuclear location sequence to construction for proximity biotinylation of RNA:DNA hybrid associated protein in cell nucleus (Figure 1A). HBD-TurboID were stable expressed in 293T (Figure 1B). After biotin incubation, the protein of HBD-TurboID 293T cell line showed significant biotinylation comparable to that of TurboID 293T cell line detected by Sa-HPR (Figure 1C). The biotinylated proteins were affinity precipitated (AP) by Sa beads and estimated by Sa-HPR. After incubation with biotin, more affinity precipitated proteins were detected for HBT-TurboID 293T cell line as well as TurboID 293T cell line comparing with that of without biotin (Figure 1D). The results showed functional biotin labeling for HBT-TurboID system.

HBD-TurboID were designed to explore R-loop associated proteins. To exclude if direct interaction of HBD-TurboID and those proteins exist, HBD-TurboID immunoprecipitation (IP) were firstly carried out and representative R-loop protein were estimated. The result showed DHX9 DDX5 as well as subcellular markers GAPDH and histone H3 were found no immunoprecipitation with HBD-TurboID protein (Figure 1E). Comparing with no biotin treatment, significantly amount of DHX9 and DDX5 instead of subcellular marker GAPDH and histone H3 were affinity precipitated by Sa beads after biotin labeling for HBD-TurboID 293T cell line (Figure 1F). HBD-TurboID system was suggested to be a efficient R-loop associated protein labeling system and its advantage was discussed in last section.

AKAP8 binding and remodulating R-loop. AKAP8 binds with both DNA and RNA. The interactome of AKAP8 contains R-loop associated proteins including RPA, hnRNPs, and DDX (Figure S1A). To investigate the relationship between AKAP8 and R-loop, we first confirmed their interaction by HBD-TurboID proximity labelling system. Extraction of HBD-TurboID 293T stable cell line incubated with biotin were affinity precipitated by Sa beads and AKAP8 was estimated in affinity precipitated product. The result showed AKAP8 was not detected in IP product of HBD-TurboID expressed cells, however was obviously detected in AP product of HBD-TurboID expressed cell after incubation with biotin (Figure 2AB). The interaction between R-loop and AKAP8 was further confirmed by S9.6 immunoprecipitation. As is shown, AKAP8 co-precipitated with S9.6 in 293T cell while homologous protein AKAP8L did not (Figure S1B). After RNase H treatment, no AKAP8 signal was showed in S9.6 IP products of 293T cell (Figure 2C). The results suggested that AKAP8 is a new revealed R-loop associated protein. We further estimated and confirmed this interaction in A549, HeLa, U2OS, and UMSC (Figure 2DF). Giving AKAP8 was reported as RNA binding protein, we also investigated whether RNA is in charge with the interaction between AKAP8 and R-loop containing RNA. Interestingly, after RNase A treatment, more AKAP8 signal seamed shown in S9.6 IP products of various cells (Figure 2DF). This may be cause by release of AKAP8 trapped by RNA and more amount of AKAP8 interaction with R-loop.

Subcellular location of AKAP8 and R-loop was subsequently to be estimated. The immunofluorescence image showed AKAP8 had mostly nuclear location, while R-

loop was also found partially nuclear location. Signal abundance distribution presented by gray value-distance showed accordingly (Figure 2E). S9.6 was reported to positively closed related to double strand break DNA represented by molecular marker rH2A.X. We also estimated subcellular distribution of AKAP8 and rH2A.X. It was imaged that AKAP8 formed speckles like rH2A.X foci. Interestingly, they showed obviously merged signal distribution according to gray value-distance analysis (Figure 2E). These results implicated nucleus colocation of AKAP8 and R-loop.

We nest explored whether AKAP8 involved in R-loop homeostasis. Relative nuclear average inter density of S9.6 was estimated in control and AKAP8 knock down 293T cell lines. The result showed AKAP8 signal of its knock down cell was significantly decreased in according with expression level, however bare differences for nuclear S9.6 signal comparing to control cell (Figure 2 GHI). R-loop level of MYC gene loci were investigated. The results showed that promoter(G4) region instead of exon loci of MYC gene accumulated R-loop (Figure 2J). These results suggested that AKAP8 was closely associated with R-loop in nuclear and contributed to its resolution in some region instead of general genome.

AKAP8 interacting with DDX5 by N terminal region containing nucleus location sequence. Previous study revealed AKAP8 interactome contains R-loop associated proteins. DDX5 was one of these proteins directly participating in R-loop resolution by its ATP dependent RNA helicase activity. To investigation association of AKAP8 and DDX5, GST pull down experiment were carried out and results showed exogeneous expressed AKAP8 co-precipitated with endogenous DDX5 both in 293T and A549 cell (Figure 3A). The estimation of AKAP8 and DDX5 interaction by exogenous expression, half endogenous expression of HA-AKAP8 DDX5-FLAG confirmed interaction of these two protein in both experiments (Figure S2AB). In addition, their interaction was found to be DNA/RNA independent implicated by treatment of benzonase nuclease for cell lysate before IP process (Figure 3B Figure S2C). Then AKAP8 and DDX5 were found to be co-precipitated in 293T cell (Figure 3C Figure S2D). GST-AKAP8 and DDX5-His were also expressed in E.coli and co-precipitation was estimated by GST pull down. DDX5-His was found to be co-precipitated with GST-AKAP8 instead of GST (Figure 3D). These results revealed the direct interaction of AKAP8 and DDX5 protein.

The subcellular location of AKAP8 and DDX5 was nest investigated. The immunofluorescence image of exogenous HA-AKAP and DDX5-FLAG of 293T cell showed that both of them had almost nucleus location. Besides, the signal profile distribution seemed to have a positive co-relation (Figure 3E). The immunofluorescence image of AKAP8 and DDX5 of A549 cell showed both of them had almost nucleus location and correlation of signal profile distribution (Figure 3). It was suggested AKAP8 and DDX5 were almost transported into nucleus and had a direct interaction.

To investigate binding domain of AKAP8 and DDX5, several truncated HA-AKAP8 and DDX5-FLAG taking their conserved domain into consideration were expressed in 293T cell. For human AKAP8 protein, it contains NMTS, two NLS, two ZNF, and PKA binding domain. For human DDX5 protein, it contains Q motif, DEAD box motif, helicase C terminal, and transactivation domain (Figure 3F). The HA IP of co-expressed truncated HA-AKAP and DDX5-FLAG gave the evidence that N terminal of

AKAP8 contain NMTS was co precipitated with DDX-FLAG. However, the FLAG IP of co expressed truncated DDX5-FLAG and full length HA-AKAP8 showed all expressed truncated DDX5-FLAG co precipitated with HA-AKAP8 (Figure 3G). It was suggested NMTS domain of AKAP8 was responsible for their interaction however DDX5 had possibly multiple regions to bind with AKAP8.

Given subcellular colocation and interaction relation, we nest investigated whether truncated HA-AKAP8 disturb DDX5-FLAG subcellular location when co express in 293T. The immunofluorescence image showed N terminal of AKAP8 containing NMTS was sufficient to satisfy nuclear location nevertheless C terminal of AKAP8 lacking NMTS and NLS domain showed cytoplasmic distribution (Figure 4H). Overexpressed DDX5-FLAG with empty HA and other truncated AKAP8 plasmid in 293T cell showed mostly nuclear sublocation excepted for only PKA binding domain deleted AKAP8. This truncated AKAP8 showed nuclear location, but the DDX5-FLAG appear to have more cytoplasmic distribution (Figure 4H). It was imaged that N terminal of AKAP8 contributed to its nuclear targeting character and NMTS domain containing region was sufficient to achieve as well as AKAP8 interaction with DDX5. The disputation of PKA binding domain of AKAP8 may perturb DDX5 nuclear targeting.

AKAP8 reduction enhancing chromatin associated DDX5. To investigate whether AKAP8 affects DDX5 expression, AKAP8 knock down 293T cell lines were established. Transcriptional and expressional level of AKAP8 was significantly reduced in two cell lines (Figure 4A-C). The expression level of DDX5 was found no significant changes (Figure 4BC). Since truncated AKAP8 may perturbed DDX5 nucleus signal, we estimated subcellular DDX5 level in fractions. The results showed that DDX5 level in cytoplasm and nucleoplasm have few changes but increasing of chromatin associated component in AKAP8 depleted cell comparing to control cell (Figure 4DE). Another known R-loop protein DHX9 has bare changes in all test cell fraction (Figure 4DF). The result implicated that reduction of AKAP8 increased chromatin associated DDX5 level.

AKAP8 playing roles in regulating oxide process of cancer cells. Given the association of AKAP8 and R-loop, and study of AKAP8 participating in splicing process, the RNA-seq by long reads method and data analysis of AKAP8 knock down cancer cell line were carried out. Comparing to control cell, differential expressed genes (DEGs) of 214 up regulated and 221 down regulated were found in shAKAP8 cell (Figure 5A Figure S3A). Tendency of relative RNA level of AKAP8 and several DEGs in two cell line were estimated by qPCR and showed accordance with reads abundance of RNA-seq (Figure 5B). Since AKAP8 was reported to play roles in RNA splice, we also investigated different expressed transcripts and alternative polyadenylation (APA). The APA motifs were analysis and listed including canonical AATAAA motif as well as CG abundance motif like CCAGCCTG (Figure S3B). The alternative splicing happened mostly by exon skipping which was over 60% of all splicing events. Other splicing ways including 5’, 3’ stie splicing ranged from about 3~13% (Figure 5D). The different splicing ways of two cell lines showed comparable percentage value suggested AKAP8 appeared to no preference for alternative splicing location in this test condition.

To comprehensively investigate roles of AKAP8 in biological metabolism and metabolic network, KEGG annotation and classification of DEGs were carried out. Classified KEGG item of upregulated and downregulated DEGs were listed respectively (Figure 5C). it was attractive that pathway in cancer item was found both in upregulated gens and downregulated genes. RNA degradation item was found only in up regulated genes while oxidative phosphorylation item was found in downregulated genes possibly contributed by transcription factor regulating pattern (Figure S3C). Gene set enrichment analysis (GSEA) of all genes were perform to achieve enrichment analysis on all genes based on the expression of all genes without prior experience . Among the GSEA item, RNA degradation item appeared to show positive enrichment score (Figure S3D). Mitochondrial respiratory chain complex I and mitophagy item related to oxidative phosphorylation pathway showed negative and positive enrichment score from comprehensive judgements respectively (Figure 5E). These GSEA character was in according with KEGG classification results. It was implicated that AKAP8 seemed to involving in RNA degradation and mitochondrial metabolism in carcinoma cell line.

AKAP8 as a potential oncogene involving in lung adenocarcinoma progress. To investigate whether AKAP8 is associated to carcinoma progress, statistical analysis of its expression across different types of cancers were carried out. As is shown, except pancreatic adenocarcinoma (PAAD), clear cell of renal cell carcinoma (RCC), and uterine corpus endometrial cancer (UCEC), AKAP8 expression in other types of carcinoma had higher score than that in normal tissue (Figure 6A). Since over expression of AKAP8 in lung carcinoma was reported in several cases but no experimental evidences were addressed, we emphasized to investigate its roles in lung carcinoma. As is shown, both of expression of AKAP8 in a lung adenocarcinoma and lung squamous cell carcinoma tissue had significantly high score than that in normal tissue (Figure 6B). High expressed AKAP8 lung carcinoma patient seemed to have lower survival probability (Figure 6C). we investigated relation of AKAP8 and lung carcinoma cell line A549. More colony of A549 with higher AKAP8 expression formed (Figure 6D). It was implicated that high expression of AKAP8 may involve in lung carcinoma. These results suggested that AKAP8 was possibly regarded as one of oncogenes for lung carcinoma.

We further performed PCA dimensionality reduction of DEGs of shCTRL and shAKAP8 in lung carcinoma of TCGA gene expression database. The results showed that expression profile of DEG set of normal tissue including lung, lung adenocarcinoma (LUAD) and lung squamous cell carcinoma (LUSC) (Figure 6E). Normal tissue aggregated in similar location of PCA 3d axis graph. expression profile of DEG set of LUAD and LUSC aggregated in distinct location. Moreover, the PCA aggregation of LUAD and LUSC separated in a 2d axis graph (PC1-PC3). This was implicated that AKAP8 may had difference effect of metabolism in LUAD and LUSC.

AKAP8 remodulating R-loop accumulation and transcription of UCP2. Previous results in this study showed AKAP8 contributed to mitochondrial metabolism. One of most regulated gene of mitochondrial associated DEGs is UCP2. We found lower survival probability was presented in UCP2 high expression patients (Figure 7A). In addition, gene expression correlation analysis of AKAP8 and UCP2 was with

significant p value (0.018) and positive R value. However, no significant correlation appeared to be found in both LUSC and normal tissue (Figure 7B). It is implicated that the positive regulation of UCP2 by AKAP8 may play roles in LUAD progress.

We estimated R-loop formation after AKAP8 depleting in A549. AKAP8 signal of its knock down cell was significantly decreased in according with expression level and nuclear S9.6 signal also reduced comparing to control cell (Figure 7C-E). We confirmed mRNA level of UCP2 significantly reduced in AKAP8 knock down A549 cell line (Figure 7G). Further the R-loop level of UCP2 gene was estimated. The results showed R-loop significant accumulated in UCP2 promoter but bare changes in exon in AKAP8 knock down cell (Figure 7FH). Together, these results suggested AKAP8 modulated R-loop of UCP2 promoter and mRNA level of UCP2 may play roles in lung adenocarcinoma progress.

Discussion

In this study, we first claimed that AKAP family member AKAP8 bind with R-loop and associated with cellular R-loop regulation. N terminal of AKAP8 was responsible for its nucleus location and interaction with DDX5, while depleted AKAP8 contributed to increasing of chromatin associated DDX5. The depletion ofAKAP8 also disturbed transcriptional profile in carcinoma cell line by regulating pathways including RNA metabolism and mitochondrial pathway. AKAP8 was predicted as positive regulator for lung carcinoma

R-loop plays critical roles in biological processes including transcription initiation/termination, DNA replication, DNA damage/repair. It is also not to be neglected in immunoglobulin gene class switch, genome instability and telomere maintenance (Petermann et al. 2022) (Niehrs and Luke 2020) (García-Muse and Aguilera 2019) (Wigton and Ansel 2021) (Toubiana and Selig 2018). So it is worthy to deeply dig function of R-loop associated proteins. Basing of R-loop antibody S9.6, researches employed pull-down subsequently mass spectrometry technology to identify R-loop proteins in various cells (Cristini et al. 2018) (Wu et al. 2021). Several groups employed inactive RNase H or HBD domain (RNA:DNA hybrid domain from RNase H), both of them capable of binding with RNA:DNA hybrid, combining proximity labeling to explore R-loop interacting proteins. HBD fusion with an engineered variant of APEX2 (ascorbate peroxidase) was employed to develop RNA:DNA proximity proteomics termed as RDProx and identify R-loop interactome (Mosler et al. 2021). Inactive RNase H (D210N, RHΔ) fused an engineered biotin ligase TurboID to identify repertoire of site specific R-loop modulators (Yan et al. 2022). However, S9.6 immunoprecipitation was restricted R-loop interactors identification under in vitro condition since the IP process was conducted by using cell extraction. For RDProx and RHΔ-TurboID method, they were beyond this problem however with their own limitation. Biotin-phenol transferase activity of APEX is dependent on H_2O_2 meaning that this system has routine of H_2O_2 incubation. This may affected redox balance of cell and triggers metabolism changes leading to R-loop and its interactors disturbance. RNase H1 is monomer in cell which provides advantage for exogenous RHΔ without bother of endogenous RNase H1 for associated protein analysis. However, as a large protein molecular instead of peptide, inactive RNase H1 has its own interactors may cover or shelter the R-loop interactors even though control experiment set.

Taking these into consideration, we employed HBD, for less instinct interactors and TurboID, for harmless proximity label for cell, to establish HBD-TurboID proximity labeling system and to label R-loop interactors. We had verified this system by labeling and detection of previous known R-loop binding protein DDX5 and DHX9. Further we identified new R-loop associated protein AKAP8 by this system (Figure 1, Figure 2). By HBD-TurboID proximity labeling and Sa affinity, we used 20% volume of cell extraction for S9.6 immunoprecipitation as affinity reaction system and achieved more obvious signal of target protein by western bloting in same experimental condition. This method for detection of weak binding R-loop protein appear to be advantageous comparing with traditional S9.6 immunoprecipitation method. Nevertheless, one thing can not be neglected that both S9.6 and HBD

397 showed slight preference for dsRNA, like 1/25 affinity preference of S9.6 binding
398 with RNA:DNA and 1/(16-127) for that of HBD (Bou-Nader et al. 2022) (Nowotny et
399 al. 2008) (Wang et al. 2021). There is possibility that R-loop interactors identified by
400 using two methods may also contain dsRNA binding proteins.
401 AKAP8 was firstly reported before thirty years but only about sixty researches
402 were indexed. In the beginning the function of AKAP8 was focused on its interacting
403 with cyclins, regulation on mRNA stability and splicing (Arsenijevic et al. 2004)
404 (Jungmann and Kiryukhina 2005) (Kvissel et al. 2007). In recent ten years, AKAP8 was
405 reported to regulation epigenetics modification of H3K4 methylation by functionally
406 association with MLL complexes and gene expression in embryonic stem cells (Jiang
407 et al. 2013) (Bieluszewska et al. 2018). Its roles in signal transduction of ERK, cAMP
408 and DNA damage was also addressed by several research groups (Asirvatham et al.
409 2021) (Kong et al. 2023) (Chan et al. 2023). It was more attractive that the function
410 of AKAP8 in tumorigenesis associated RNA splicing regulated by its phase-liquid
411 separation. Expression of AKAP8 was reported to be positively associated with
412 growth of breast cancer cell maybe by possibility of regulation of inflammatory
413 response and apoptosis gene expression as well as regulation of splicing for
414 tumorigenesis gene (Li et al. 2020a). Another report showed that AKAP8 antagonized
415 with splicing activity of hnRNPM to prevent EMT (epithelial-mesenchymal
416 transition)-promoting splicing in breast cancer cell (Hu et al. 2020). N terminal IDR
417 (intrinsically disordered region) 101-210aa of AKAP8 especial Tyr site was regarded
418 as the pivot site responsible for phase-liquid dynamic status in nucleus. Mutation of
419 IDR Tyr or deletion of IDR changed phase-liquid balance of nucleus AKAP8 in
420 carcinoma cell resulting in disturb of RNA splicing (Li et al. 2020a). N terminal region
421 1-100 aa of AKAP8 was reported to interact with RNA processing proteins including
422 splicing factors, RNA helicase and hnRNP by HA IP MS method (Hu et al. 2016).
423 Therefore, N terminal of AKAP8 was regarded as key region for RNA splicing
424 regulation. This region was founded to dominate AKAP8 nucleus distribution as well
425 as interaction with DDX5(Figure 4). However, whether this region is sufficient to
426 regulate biofunction of DDX5 in cell is still needed to be determined.
427 AKAP8 contains two ZF (zinc finger)domains in its middle region proposed
428 function including mediation of chromatin condensation and RNA motif binding
429 (Collas et al. 1999) (Hu et al. 2016). These motif was supposed to involve in RNA
430 splicing by direct binding with pre-mRNA. We demonstrated that AKAP8 bind with R-
431 loop and regulated its level in carcinoma cell line (Figure 2, Figure 7). It was
432 suggested that complicated regulatory function of AKAP8 in RNA splicing. moreover,
433 R-loop has interference with splicing process. The fact AKAP8 associating with R-loop
434 and regulating its level make it as a more complicated mechanism.
435 There is less doubt that AKAP8 is closely related to tumorigenesis and progress.
436 Knock down of AKAP8 significantly reduced cell growth and tumorigenicity of breast
437 carcinoma (Li et al. 2020a). AKAP8 was considered as suppressor of tumor metastasis
438 by antagonizing EMT process (Hu et al. 2020). dynamically interacted with Cx43
439 (connexin 43) and competitively separated from cyclinE1/E2 to regulate G1/S
440 conversion in lung carcinoma cells (Chen et al. 2020) (Chen et al. 2016). Our
441 experiment also revealed that AKAP8 contributed to cell growth of lung carcinoma
442 cell line (Figure). Besides, Transforming growth factor beta(TGF-beta) is considered
443 one of most main driver of fibrosis in progressive interstitial lung disease IPF

(Idiopathic pulmonary fibrosis) (Young et al. 2023). RNA-seq results showed that knock down of AKAP8 disturbed TGF-beta/SMAD3 regulating patten (Figure S3C). The regulation of TGF-beta by AKAP8 was also reported in previous research (Li et al. 2020a). Therefore, it is not to be neglected the roles of AKAP8 in lung disease.

In this study, we offered evidence that knock down of AKAP5 increased nucleus DDX5 level. DDX5 as a prognostic marker involves in proliferation and tumorigenesis of NSCLC (non-small cell lung cancer) cells through activating the β-catenin signaling pathway (Wang et al. 2015). Further evidence showed depletion of DDX5 reduced growth and mitochondrial dysfunction in chemoresistant SCLC (small cell lung cancer) cell line by possibility of reduction of intracellular succinate which serves as direct electron donor to mitochondrial (Xing et al. 2020). DDX5 reduced expression in various cancer cell lines and tumor xenografts under hypoxia condition and rescued DDX5 in hypoxia showed R-loop levels accumulation further (Leszczynska et al. 2023). The resolution activation of DDX5 on R-loop in cell was reported only years ago and several co-regulators were also focused in recently as introduced in this text. post translation modification of DDX5 impaired its biofunction in R-loop regulation. RGG/RG motif of DDX5 methylated by protein arginine methyltransferase 5 (PRMT5) was not necessary for R-loop resolution activity but was required for interacting of DDX5 with XRN2 exoribonuclease to resolve R-loop (Mersaoui et al. 2019). DDX5 was phosphorylated at tyrosine residue in cell and was a cellular target of p38 MAP kinase. The phosphorylation of DDX5 showed effects on its RNA unwinding activity (Yang et al. 2005). DDX5 was also physiological substrate of PAK5 (P21-activated kinase 5) phosphorylated DDX5 at Thr69. DDX5-phosphorylation-mediated lysine 53 (K53) SUMOylation enhanced DDX5 stability and both two modification of DDX5 facilitated Drosha/DGCR8/DDX5 complex formation (Li et al. 2021). However there was no direct evidence that phosphorylation of DDX5 involved in R-loop resolution. AKAP8 is kinase anchoring protein and associated with kinase subcellular spatial orientation. Whether AKAP8 interacting with DDX5 direct DDX5 phosphorylation and play roles in regulating cellular R-loop level is an attractive question. It is also interesting that DDX5 interacted with UCP2 in NSCLC cells and affected tolerance of cell to chemotherapy drugs by AKT/mTOR signaling (Yang et al. 2021). In this study, we speculated that UCP2 transcription was down regulated but R-loop level of DD5 gene promoter was up regulated by knock down of AKAP8 in carcinoma cell line (Figure). Therefore, AKAP8, DDX5, R-loop and UCP2 showed a complex regulating net to modeling metabolism of lung carcinoma cell.

481 **Material and method**
482
483 **Cell and cell culture.** HEK293T human embryonic kidney, A549 human lung
484 adenocarcinoma, HeLa human ovarian carcinoma, U2OS human osteosarcoma cell
485 lines and UMSC umbilical cord mesenchymal stem cell were used in this study.
486 Generally, cell were cultured in DMEM medium supplemented with 10% fetal bovine
487 serum, 1% penicillin/streptomycin in at 37°C in a humidified atmosphere with 5%
488 CO_2. Cell were cultured to a confluence of about 90% and then passage by 1:3~5 to
489 fresh complete medium. Cells were regularly confirmed mycoplasma free before
490 experiment.
491
492 **Plasmid construction.** pLKO.1-TRC-shRNA plasmid were constructed by
493 restriction enzyme digestion and ligation. Oligo of hair pin shRNA of AKAP8
494 containing flanking Age I and EcoR I enzyme site sequence were synthesized (shCTRL
495 oligo: 5'3'; shAKAP8-CDS oligo: 5'
496 CCGGGCCAAGATCAACCAGCGTTTGCTCGAGCAAACGCTGGTTGATCTTGGCTTTTTG3', 5'
497 AATTCAAAAAGCCAAGATCAACCAGCGTTTGCTCGAGCAAACGCTGGTTGATCTTGGC3';
498 shAKAP8-3'UTR oligo:
499 5'CCGGGCTGAAGTACATTGTCCTTAGCTCGAGCTAAGGACAATGTACTTCAGCTTTTTG3',
500 5'AATTCAAAAAGCTGAAGTACATTGTCCTTAGCTCGAGCTAAGGACAATGTACTTCAGC3').
501 The sense and antisense oligo were mixed and heated to 95℃ and annealed to base
502 pair complementary by immediately transfer to ice or programmed gradient cooling
503 to 25℃. pLKO.1-TRC-shRNA empty plasmid were digested by Age I and EcoR I,
504 recycled and ligated with annealed shRNA oligo. pLKO.1-SHC002 (Sigma-Aldrich,
505 #SHC002) was as control shRNA plasmid.
506 Expression plasmid were generally constructed by seamless method or blunt
507 end ligation. pCR3.1 backbone, AKAP8 with plasmid flanking overlap sequence were
508 amplified and then homologous recombination according to guide of seamless kit
509 instruction to construct pCR3.1-HA-AKAP8. Truncated HA-AKAP8 expression plasmid
510 were constructed by PCR amplified using pCR3.1-HA-AKAP8 as template and blunt
511 end ligation. pCMV3-DDX5-FLAG were bought from Sino Biological company
512 (#HG16175-CF). Truncated DDX5-FLAG expression plasmid were constructed by PCR
513 and blunt end ligation.
514 pGEX-4T-AKAP8 expressing GST-AKAP8, and pET28a-DDX5 expressing His-DDX5
515 were also constructed by seamless method. The truncated expression plasmid were
516 constructed by PCR and blunt end ligation.
517 pLV3-CMV-TurboID-NLS-FLAG were originally bought from MiaoLingBio
518 company. Kozak sequence were added after CMV before TurboID and used to
519 construct HBD-TurboID plasmid. HBD with overlap sequence and pLV3-TurboID-NLS-
520 FLAG backbone plasmid were amplified to homologous recombined as pLV3-HBD-
521 TurboID-NLS-FLAG.
522
523 **Lentivirus package and infection.** 293T cell were passage and cultured over night
524 to confluence of 80% in 6 well plate. The cell transfection were carried out for
525 lentivirus package by using following plasmid: 1 μg pLKO.1-shRNA, 0.75 μg psPAX2,
526 0.25 μg pMD2.G mixed in 100 μL FBS free DMEM medium. 4 ug PEI in equal volume
527 DMEM was added into plasmid and gently mixed, incubated for 10 min at room

528 temperature. Mixture of plasmid and PEI were dropwise addition to transfect 293T
529 cell. Virus were harvested after 48 h. For infection, target cell were passage and
530 cultured over night to confluence of 80% in 6 well plate. Medium were discarded and
531 1 mL virus and 1 mL fresh complete medium were added with mixture of final
532 concentration of 8 μg/mL polybrene. Medium was replaced by 2 μg/mL Puro
533 medium after 48 h culture. The selection were lasted at least for 5 days for stable
534 cell line.
535
536 **Biotin labelling and Sa affinity precipitation.** Biotin stock was prepared at
537 concentration of 100 mM in dimethyl sulfoxide (DMSO). The cell were cultured to
538 confluence about 90%. Biotin stock was diluted by serum medium and directly added
539 to medium at final concentration of 500 μM for 10 min unless indicated otherwise.
540 To terminating the label proceed, cell was transferred to ice, discarding the medium
541 and washed by pre frozen PBS for 3 times. The cell was scraped from plate and
542 harvest by centrifuging under 4°C 500 g for 5 min. Supernatant was removed. The
543 pellet of about 10^7 cell was resuspended and lysed by 1 mL WCE buffer (50 mM Tris
544 pH 8.0, 150 mM NaCl, 0.5% NP-40, 1 mM EDTA and 10% glycerol). After 15 min
545 rotation in 4oC refrigerator, whole cell lysate (WCL) was clarified by centrifuging 4°C
546 12000 g for 10 min. The total protein concentration of WCL was estimated by BCA
547 protein assay. WCL containing 0.2 mg protein was incubated with 15 μL Sa magbeads
548 for 1.5 h rotation under 4°C. Beads was subsequently washed twice by WCE buffer,
549 once by 1 M KCl, once by 0.1 M Na2CO3, once by 2 M urea/10 mM Tirs pH 8.0,
550 recovered by twice WCE buffer washing. For western blotting, the slurry was boiled
551 at 95°C for 5~10 min by adding 30 μL 1*loading buffer.
552
553 **RNA:DNA hybrid (R-loop) associated protein immunoprecipitation.** R-loop
554 associated protein of cell was precipitated by S9.6 referring to previous reports.
555 Briefly, 10^7 cell were harvest and washed twice by pre cold PBS. 1 mL WCL buffer
556 was added and fully suspended by vortex following 30 min incubation on ice. After
557 high speed centrifugation, supernatant were collected for IP. Antibody was
558 incubated for 2 h with 15 μL pre balanced proteinA/G beads in 100 μL WCL buffer
559 per IP reaction. 500 μL WCL was added into beads and incubated for 2 h in 4°C
560 condition with gently upside down mix. Beads were separated and supernatant was
561 discarded. Beads was washed by 500 μL WCL for 3 min at least 6 times. The beads
562 slurry was resuspended by 30 μL SDS-loading buffer and boiled under 95°C for 10
563 min. the IP products was separated by SDS-PAGE and target protein was estimated
564 by western blotting. For RNase H or RNase A test group, 5U RNase H or 10 ug RNase
565 A were added per IP reaction and incubated at 37℃ overnight.
566
567 **Immunofluorescence.** Cell was cultured into confluence about 90% and
568 enzymatic digested by trypsin, seeded by 1:5 in 6 or 12 well plate before 24h of
569 immunofluorescence. The 20 mm slide was pre-autoclaved and placed in well before
570 seeding cell. For transfecting, cell was seed by 1:8 and cultured for 24 h. Transfecting
571 of cells was conducted according to method mentioned in this section. After 36 h
572 culture, the following operation was carried out. The plate was washed by PBS, fixed
573 by 4% PFA for 15 min, stop fixation process by 2mg/mL Glycine for 10 min twice,
574 permeated by 0.2% Triton X-100 for 10 min. following PBS washing twice, cells were

575 blocked by 3% BSA/PBS for 1h at room temperature. After PBS washing thrice, cells
576 were incubated with primary antibody diluted by 3% BSA/PBS for 1 h at room
577 temperature. After washing thrice by wash buffer (1% BSA, 0.05% Tween 20, PBS)
578 thrice, cells were incubated with fluorescence labeled second antibody for 1 h. After
579 washing thrice by wash buffer, cells were incubated with DAPI for DNA stain. The
580 slide were sealed for imaging by Nikon A1. For R-loop immunofluorescence, cell
581 were fixed and permeated by pre-cold methanol for 10 min at -20℃ and acetone for
582 1 min at room temperature. After washing thrice by PBS, the cells were blocked and
583 incubated with antibody.
584
585 **Antibody used in this study.** S9.6 (Merck, #MABE1095), anti-AKAP8 (Zenbio,
586 #R26398), anti-AKAP8L (Zenbio, #160665), anti-DDX5 (Cell signaling technology,
587 #9877; Proteintech, #67025-1-Ig), anti-DHX9 (Zenbio, #382331), anti-H2A.X (Zenbio,
588 #201082-7G9), anti-FLAG (Sigma-Aldrich, #F1804; Proteintech, #80010-1-RR), anti-
589 HA (Proteintech, # 66006-2-Ig), anti-GAPDH (Proteintech, #60004-1-Ig), anti-H3
590 (Proteintech, #68345-1-Ig), Normal Rabbit IgG (Cell signaling technology, #2729),
591 Mouse IgG (Proteintech, # B900620), HRP-Goat antibody (Proteintech, SA00001-2,
592 SA00001-3), fluorescence crosslinked donkey antibody (Proteintech, # SA00013-5,
593 SA00013-6, SA00013-7, SA00013-8).
594
595 **DRIP to enrich R-loop DNA.** Cells were cultivated into confluence of 90% and
596 medium were discard. Cells were washed by PBS twice and scraped from dish placing
597 on ice. After centrifugation at 4℃ 500g for 5 min, 10 cm dish cultivated or 10^7 cell
598 were harvested and resuspended by 0.5 mL lysis buffer (10mM Tris pH 8.0, 1% SDS,
599 2mM EDTA, 100mM NaCl) with 50 µLg/mL Protein K. after incubation at 37℃
600 overnight, final concentration of 20 ug/mL RNase A (DNase free) were added and
601 incubated for 30 min. Add one volume phenol/chloroform extract liquid, vertex and
602 rest for 10 min at room temperature. Transfer to phase gel lock tube and
603 centrifugate at 12000 rpm for 5 min, transfer liquid to new tube. Add 1/10 volume 3
604 M NaAc (pH 5.2) and 2 volume alcohol. After DNA depositing at -20℃ for at least 30
605 min, centrifugate at 12000 rpm for 10 min and discard supernatant. DNA was
606 resuspended by 1 mL 80% alcohol and then centrifugated at 10000 rpm for 10 min.
607 supernatant was aspirated totally and DNA was air-dried. About 1 mL TE buffer (10
608 mM Tris–HCl pH 8.0, 1 mM EDTA) was added and DNA was totally resolved for DNA
609 concentration measurement. Diluted DNA concentration to 0.5 mg/mL. DNA was
610 fragmented into 200-1000 bp by ultrasonication. 300 µL DNA (150 µg) was placed in
611 sonication tube (Diagenode, Bioruptor Pico). The parameter of sonication instrument
612 was set at 4℃ 15 s/45 s (work/off) for 8 cycles. 50 ug DNA fragment was diluted by
613 IP buffer (10 mM Na_2HPO_4 pH 7.0, 140 mM NaCl, 0.05 % Triton X-100) to 500 µL was
614 used for DRIP. 15 µL Protein A/G beads used for one DRIP sample. Protein A/G beads
615 was pre-blocked by 0.5% BSA/PBS for 2 h and washed by IP buffer for twice. Protein
616 A/G beads was incubated with 2 ug S9.6 in 100 mL IP buffer at 4℃ for 2 h by upside
617 down mix. 50 µg DNA fragment was diluted by IP buffer up to 500 mL. S9.6 protein
618 A/G beads suspend slurry was added into DNA fragment. Before this, 5 µL DNA was
619 aspirated as input. The IP component was mixed by gently upside down at 4℃ for 2
620 h. beads slurry was separated and supernatant was aspirated. Beads slurry was
621 washed with 1 mL IP buffer over five times. the beads slurry was resuspended by 200

622 µL PK buffer (50 mM Tris–HCl pH 8.0, 10 mM EDTA, 0.5 % SDS) with 1 µL 20 mg/mL
623 protein K and incubated at 55℃ for 4 h. IP DNA and input diluted by IP to total
624 volume of 200 µL was purified by phenol/chloroform protocol mentioned in this
625 method. Purified DNA was resolved by 50 µL TE buffer for further experiment.
626
627 **Full length transcriptome.** Cells were cultured to influence of 90% in 6 well plate.
628 Medium was discard and cells were washed by PBS twice. 1 mL TRIZOL was added
629 for lysis of cell. The lysate was transferred to tube and incubated at room
630 temperature for 5 min. 0.2 mL chloroform was added and drastic mixed and then
631 placed for 10 min. One volume of isopropanol was added and mixed upside down.
632 after centrifugation of 12000 rpm for 10 min, two volume alcohol was added to
633 supernatant. After DNA depositing at -20℃ for at least 30 min, centrifugate at 12000
634 rpm for 10 min and discard supernatant. DNA was resuspended by 1 mL 80% alcohol
635 and then centrifugated at 10000 rpm for 10 min. Supernatant was aspirated totally
636 and DNA was air-dried. 50 µL distill water was added to resuspend total RNA at 65℃
637 for 10 min. Oxford Nanopore Technologies(ONT) full length RNA-seq and analysis
638 was carried out by Biomarker Technologies Co., LTD.
639
640 **qPCR.** cDNA was synthesized by reverse transcription using of 1µg total RNA as
641 template according to manufacture instrument of HiScript III RT SuperMix for qPCR
642 (Vazyme, #R323-01). cDNA was generally diluted 10 fold by distill water. For IP DNA
643 qPCR, DNA was resuspended in 50 µL distill water. qPCR was carried out using of PCR
644 mix, DNA template, primer according manufacture instruments of TB Green Fast
645 qPCR Mix (Takara, #RR430) and CFX96 Real-Time System (BIO-RAD, C1000 Touch).
646 The Ct value was used for relative abundance calculation by $2^{(-\Delta\Delta Ct)}$ method.
647
648 **Cell colony formation.** Cell were cultured in complete medium to logarithmic
649 phase and enzymic digested from dish. Cell were then inoculated in 6 well plate by
650 1000 cell per well. After 24 h, plasmid were transfected by PEIpro and medium were
651 refreshed after 24 h. cell were continue cultured for another 10 days. Medium were
652 discarded and cell were washed by PBS twice. Cell were fixed by adding 1 mL
653 methanol for 30 min. methanol was discarded and cell were stained by 0.1% crystal
654 violet for 3 min. Plate were washed by PBS to clear for cell colony imaging.
655
656 **Isolation of cytoplasm, nucleoplasm, chromatin associated fraction.** 10^7
657 cultured in 10 cm dish was washed by pre-cold PBS twice. Cells were scraped and
658 harvested by centrifugation at 4℃ 500g for 5min. Cells were resuspended by 0.5 mL
659 cytoplasmic lysis buffer (50 mM Tris-HCl pH 8.0, 140 mM NaCl, 1.5 mM $MgCl_2$, 0.5%
660 NP-40, 1 mM DTT and protease inhibitor) and lysed for 5 min in ice. After
661 centrifugation of 800 g for 2 min at 4℃, supernatant was harvested as cytoplasmic
662 fraction after high speed centrifugation. The pellet was washed by cytoplasmic lysis
663 buffer without NP-40, centrifuged and then resuspended in 50 µL nucleoplasmic lysis
664 buffer 1 (20 mM Tris-HCl pH 7.9, 75 mM NaCl, 0.5 mM EDTA and 50% (v/v) glycerol)
665 totally. 0.5 mL pre-cold nucleoplasmic lysis buffer 2 (20 mM HEPES-KOH pH 7.6, 300
666 mM NaCl, 0.2 mM EDTA, 7.5 mM $MgCl_2$, 1% (v/v) NP-40, 1 M urea and protease
667 inhibitor) was added to suspension, vortexed and incubated for 15 min on ice. The
668 supernatant was gently harvested by centrifugation at 4℃ 2000 g for 4 min as

669 nucleoplasmic fraction after high speed centrifugation. The pellet was quickly
670 washed by nucleoplasmic lysis buffer 2 and harvested by centrifugation of 13000 g at
671 4℃ for 4 min. the supernatant was discarded and pellet was resuspended by 0.5 mL
672 high salt buffer (50 mM Tis pH 8.0, 500 mM NaCl and protease inhibitor) with 250 U
673 Turbo DNase and incubated for 30 min at 37℃ as chromatin associated fraction.
674
675 **Bioinformatic analysis and statistics analysis.** Statistic expression of AKAP8 and
676 graph plot in pan-cancer/normal tissue and different types of lung cancer/normal
677 tissue were analyzed by UALCAN platform. Correlation between gene and survival in
678 lung cancer were analyzed by Kaplan-Meier Plotter with default parameters.
679 Dimensionality reduction of DEG set from RNA-seq, gene correlation, and graphic
680 plotting were analyzed by GEPIA2 platform. T-test and p value were estimated by
681 Graphpad Prism 9.
682

Compliance and ethics

The author(s) declare that they have no conflict of interest.

Acknowledgements

This work was supported by the National Natural Science Foundation of China (31900655). It was grateful to Feng Zhou (Guangzhou Laboratory) for regent ordering, Ms. Lanlan Zhang (Guangzhou Laboratory) for help of confocal microscope operation, Dr. Yaping Chen (Chinese Academy of Science) for kind gift of pCR3.1-HA-AKAP8 plasmid, Ms. Di Wu (Guangzhou Medical University) for kind gift of UMSC cell extraction, Ms. Lin Lu and Prof. Yan Wang (Sun Yat-sen University) for funding (31900655) managements.

Reference:

Arsenijevic, T., Degraef, C., Dumont, J.E., Roger, P.P., Pirson, I. (2004). A novel partner for D-type cyclins: protein kinase A-anchoring protein AKAP95 378, 673–679.

Asirvatham, A.L., Schworer, C.M., Stahl, R., Heitzman, D., Carey, D.J. (2021). Role of A-kinase anchoring proteins in cyclic-AMP-mediated Schwann cell proliferation 83, 109977.

Bieluszewska, A., Weglewska, M., Bieluszewski, T., Lesniewicz, K., Poreba, E. (2018). PKA -binding domain of AKAP 8 is essential for direct interaction with DPY 30 protein 285, 947–964.

Boque-Sastre, R., Soler, M., Oliveira-Mateos, C., Portela, A., Moutinho, C., Sayols, S., et al. (2015). Head-to-head antisense transcription and R-loop formation promotes transcriptional activation 112, 5785–5790.

Bou-Nader, C., Bothra, A., Garboczi, D.N., Leppla, S.H., Zhang, J. (2022). Structural basis of R-loop recognition by the S9.6 monoclonal antibody 13, 1641.

Chakraborty, P., Huang, J.T.J., Hiom, K. (2018). DHX9 helicase promotes R-loop formation in cells with impaired RNA splicing 9, 4346.

Chan, D.K.H., Mandal, A., Hester, S., Yu, Z., Higgins, G.S., Kessler, B.M., et al. (2023). Biallelic FBXW7 knockout induces AKAP8-mediated DNA damage in neighbouring wildtype cells 9, 200.

Chen, P.B., Chen, H.V., Acharya, D., Rando, O.J., Fazzio, T.G. (2015). R loops regulate promoter-proximal chromatin architecture and cellular differentiation 22, 999–1007.

Chen, R., Chen, Y., Yuan, Y., Zou, X., Sun, Q., Lin, H., et al. (2020). Cx43 and AKAP95 regulate G1/S conversion by competitively binding to cyclin E1/E2 in lung cancer cells 11, 1594–1602.

Chen, X., Kong, X., Zhuang, W., Teng, B., Yu, X., Hua, S., et al. (2016). Dynamic changes in protein interaction between AKAP95 and Cx43 during cell cycle progression of A549 cells 6, 21224.

Clister, T., Greenwald, E.C., Baillie, G.S., Zhang, J. (2019). AKAP95 Organizes a Nuclear Microdomain to Control Local cAMP for Regulating Nuclear PKA 26, 885-891.e4.

Collas, P., Le Guellec, K., Taskén, K. (1999). The A-kinase-anchoring protein AKAP95 is a multivalent protein with a key role in chromatin condensation at mitosis 147, 1167–1180.

Cristini, A., Groh, M., Kristiansen, M.S., Gromak, N. (2018). RNA/DNA Hybrid Interactome Identifies DXH9 as a Molecular Player in Transcriptional Termination and R-Loop-Associated DNA Damage 23, 1891–1905.

Crow, Y.J., Manel, N. (2015). Aicardi-Goutières syndrome and the type I interferonopathies 15, 429–440.

Cui, Y., Hunt, A., Li, Z., Birkin, E., Lane, J., Ruge, F., et al. (2021). Lead DEAD/H box helicase biomarkers with the therapeutic potential identified by integrated bioinformatic approaches in lung cancer 19, 261–278.

García-Muse, T., Aguilera, A. (2019). R Loops: From Physiological to Pathological Roles 179, 604–618.

Groh, M., Gromak, N. (2014). Out of balance: R-loops in human disease 10, e1004630.

741 Grunseich, C., Wang, I.X., Watts, J.A., Burdick, J.T., Guber, R.D., Zhu, Z., et al. (2018).
742 Senataxin Mutation Reveals How R-Loops Promote Transcription by Blocking DNA
743 Methylation at Gene Promoters 69, 426-437.e7.
744 Hu, J., Khodadadi-Jamayran, A., Mao, M., Shah, K., Yang, Z., Nasim, M.T., et al.
745 (2016). AKAP95 regulates splicing through scaffolding RNAs and RNA processing
746 factors 7, 13347.
747 Hu, X., Harvey, S.E., Zheng, R., Lyu, J., Grzeskowiak, C.L., Powell, E., et al. (2020). The
748 RNA-binding protein AKAP8 suppresses tumor metastasis by antagonizing EMT-
749 associated alternative splicing 11, 486.
750 Jarnaess, E., Stokka, A.J., Kvissel, A.-K., Skålhegg, B.S., Torgersen, K.M., Scott, J.D., et
751 al. (2009). Splicing factor arginine/serine-rich 17A (SFRS17A) is an A-kinase anchoring
752 protein that targets protein kinase A to splicing factor compartments 284, 35154–
753 35164.
754 Jiang, H., Lu, X., Shimada, M., Dou, Y., Tang, Z., Roeder, R.G. (2013). Regulation of
755 transcription by the MLL2 complex and MLL complex-associated AKAP95 20, 1156–
756 1163.
757 Jungmann, R.A., Kiryukhina, O. (2005). Cyclic AMP and AKAP-mediated targeting of
758 protein kinase A regulates lactate dehydrogenase subunit A mRNA stability 280,
759 25170–25177.
760 Kang, H.J., Eom, H.-J., Kim, H., Myung, K., Kwon, H.M., Choi, J.H. (2021). Thrap3
761 promotes R-loop resolution via interaction with methylated DDX5 53, 1602–1611.
762 Kannan, A., Cuartas, J., Gangwani, P., Branzei, D., Gangwani, L. (2022). Mutation in
763 senataxin alters the mechanism of R-loop resolution in amyotrophic lateral sclerosis
764 4 145, 3072–3094.
765 Kim, S., Kang, N., Park, S.H., Wells, J., Hwang, T., Ryu, E., et al. (2020). ATAD5 restricts
766 R-loop formation through PCNA unloading and RNA helicase maintenance at the
767 replication fork 48, 7218–7238.
768 Kong, X., An, P., Xu, J., Liu, W., Lin, F., Yang, Y. (2023). A-Kinase Anchor Protein 95 Is
769 Involved in ERK1/2-Elk-1 Signal Transduction in Colon Cancer 2023, 8242646.
770 Kubota, S., Morii, M., Yuki, R., Yamaguchi, N., Yamaguchi, H., Aoyama, K., et al.
771 (2015). Role for Tyrosine Phosphorylation of A-kinase Anchoring Protein 8 (AKAP8) in
772 Its Dissociation from Chromatin and the Nuclear Matrix 290, 10891–10904.
773 Kvissel, A.-K., Ørstavik, S., Eikvar, S., Brede, G., Jahnsen, T., Collas, P., et al. (2007).
774 Involvement of the catalytic subunit of protein kinase A and of HA95 in pre-mRNA
775 splicing 313, 2795–2809.
776 Langeberg, L.K., Scott, J.D. (2005). A-kinase-anchoring proteins 118, 3217–3220.
777 Leszczynska, K.B., Dzwigonska, M., Estephan, H., Moehlenbrink, J., Bowler, E.,
778 Giaccia, A.J., et al. (2023). Hypoxia-mediated regulation of DDX5 through decreased
779 chromatin accessibility and post-translational targeting restricts R-loop accumulation
780 17, 1173–1191.
781 Li, W., Hu, J., Shi, B., Palomba, F., Digman, M.A., Gratton, E., et al. (2020a).
782 Biophysical properties of AKAP95 protein condensates regulate splicing and
783 tumorigenesis 22, 960–972.
784 Li, Y., Song, Y., Xu, W., Li, Q., Wang, X., Li, K., et al. (2020b). R-loops coordinate with
785 SOX2 in regulating reprogramming to pluripotency 6, eaba0777.

786 Li, Y., Xing, Y., Wang, X., Hu, B., Zhao, X., Zhang, H., et al. (2021). PAK5 promotes RNA
787 helicase DDX5 sumoylation and miRNA-10b processing in a kinase-dependent
788 manner in breast cancer 37, 110127.
789 Lim, Y.W., Sanz, L.A., Xu, X., Hartono, S.R., Chédin, F. (2015). Genome-wide DNA
790 hypomethylation and RNA:DNA hybrid accumulation in Aicardi-Goutières syndrome
791 4, e08007.
792 Linder, P., Jankowsky, E. (2011). From unwinding to clamping - the DEAD box RNA
793 helicase family 12, 505–516.
794 Martins, S., Eikvar, S., Furukawa, K., Collas, P. (2003). HA95 and LAP2 beta mediate a
795 novel chromatin-nuclear envelope interaction implicated in initiation of DNA
796 replication 160, 177–188.
797 Mersaoui, S.Y., Yu, Z., Coulombe, Y., Karam, M., Busatto, F.F., Masson, J.-Y., et al.
798 (2019). Arginine methylation of the DDX5 helicase RGG/RG motif by PRMT5
799 regulates resolution of RNA:DNA hybrids , 20.
800 Mosler, T., Conte, F., Longo, G.M.C., Mikicic, I., Kreim, N., Möckel, M.M., et al.
801 (2021). R-loop proximity proteomics identifies a role of DDX41 in transcription-
802 associated genomic instability 12, 7314.
803 Nie, X., Zhao, C., Zhang, Y., Huang, W., Zhou, Y., Liu, H., et al. (2023). Nucleolar
804 protein treacle ribosome biogenesis factor 1 maintains gastric cancer cell
805 proliferation by regulating R-loop associated DNA replication stress 38, 1170–1180.
806 Niehrs, C., Luke, B. (2020). Regulatory R-loops as facilitators of gene expression and
807 genome stability 21, 167–178.
808 Nowotny, M., Cerritelli, S.M., Ghirlando, R., Gaidamakov, S.A., Crouch, R.J., Yang, W.
809 (2008). Specific recognition of RNA/DNA hybrid and enhancement of human RNase
810 H1 activity by HBD 27, 1172–1181.
811 Petermann, E., Lan, L., Zou, L. (2022). Sources, resolution and physiological relevance
812 of R-loops and RNA-DNA hybrids 23, 521–540.
813 Polenkowski, M., Allister, A.B., Burbano de Lara, S., Pierce, A., Geary, B., El Bounkari,
814 O., et al. (2023). THOC5 complexes with DDX5, DDX17, and CDK12 to regulate R loop
815 structures and transcription elongation rate 26, 105784.
816 Refaat, A.M., Nakata, M., Husain, A., Kosako, H., Honjo, T., Begum, N.A. (2023).
817 HNRNPU facilitates antibody class-switch recombination through C-NHEJ promotion
818 and R-loop suppression 42, 112284.
819 Renaudin, X., Lee, M., Shehata, M., Surmann, E.-M., Venkitaraman, A.R. (2021).
820 BRCA2 deficiency reveals that oxidative stress impairs RNaseH1 function to cripple
821 mitochondrial DNA maintenance 36, 109478.
822 Ribeiro de Almeida, C., Dhir, S., Dhir, A., Moghaddam, A.E., Sattentau, Q., Meinhart,
823 A., et al. (2018). RNA Helicase DDX1 Converts RNA G-Quadruplex Structures into R-
824 Loops to Promote IgH Class Switch Recombination 70, 650-662.e8.
825 Ruiz, J.F., Gómez-González, B., Aguilera, A. (2011). AID induces double-strand breaks
826 at immunoglobulin switch regions and c-MYC causing chromosomal translocations in
827 yeast THO mutants 7, e1002009.
828 Saha, S., Yang, X., Huang, S.-Y.N., Agama, K., Baechler, S.A., Sun, Y., et al. (2022).
829 Resolution of R-loops by topoisomerase III-β (TOP3B) in coordination with the DEAD-
830 box helicase DDX5 40, 111067.

Tan, S.L.W., Chadha, S., Liu, Y., Gabasova, E., Perera, D., Ahmed, K., et al. (2017). A Class of Environmental and Endogenous Toxins Induces BRCA2 Haploinsufficiency and Genome Instability 169, 1105-1118.e15.
Thomas, M., White, R.L., Davis, R.W. (1976). Hybridization of RNA to double-stranded DNA: formation of R-loops 73, 2294–2298.
Toubiana, S., Selig, S. (2018). DNA:RNA hybrids at telomeres - when it is better to be out of the (R) loop 285, 2552–2566.
Wang, K., Wang, H., Li, C., Yin, Z., Xiao, R., Li, Q., et al. (2021). Genomic profiling of native R loops with a DNA-RNA hybrid recognition sensor 7, eabe3516.
Wang, Z., Luo, Z., Zhou, L., Li, X., Jiang, T., Fu, E. (2015). DDX5 promotes proliferation and tumorigenesis of non-small-cell lung cancer cells by activating β-catenin signaling pathway 106, 1303–1312.
Wigton, E.J., Ansel, K.M. (2021). Noncoding RNAs in B cell responses 18, 633–639.
Wu, G., Xing, Z., Tran, E.J., Yang, D. (2019). DDX5 helicase resolves G-quadruplex and is involved in *MYC* gene transcriptional activation 116, 20453–20461.
Wu, T., Nance, J., Chu, F., Fazzio, T.G. (2021). Characterization of R-Loop–Interacting Proteins in Embryonic Stem Cells Reveals Roles in rRNA Processing and Gene Expression 20, 100142.
Xing, Z., Russon, M.P., Utturkar, S.M., Tran, E.J. (2020). The RNA helicase DDX5 supports mitochondrial function in small cell lung cancer 295, 8988–8998.
Xing, Z., Wang, S., Tran, E.J. (2017). Characterization of the mammalian DEAD-box protein DDX5 reveals functional conservation with S. cerevisiae ortholog Dbp2 in transcriptional control and glucose metabolism 23, 1125–1138.
Yan, Q., Wulfridge, P., Doherty, J., Fernandez-Luna, J.L., Real, P.J., Tang, H.-Y., et al. (2022). Proximity labeling identifies a repertoire of site-specific R-loop modulators 13, 53.
Yang, L., Lin, C., Liu, Z.-R. (2005). Signaling to the DEAD box--regulation of DEAD-box p68 RNA helicase by protein phosphorylations 17, 1495–1504.
Yang, Z., Li, G., Zhao, Y., Zhang, L., Yuan, X., Meng, L., et al. (2021). Molecular Insights into the Recruiting Between UCP2 and DDX5/UBAP2L in the Metabolic Plasticity of Non-Small-Cell Lung Cancer 61, 3978–3987.
Young, O.N., Bourke, J.E., Widdop, R.E. (2023). Catch your breath: The protective role of the angiotensin AT2 receptor for the treatment of idiopathic pulmonary fibrosis 217, 115839.

867 **Figure and table legends.**
868
869 **Figure 1. Proximity labelling of R-loop associated protein by HBD-TurboID.** A,
870 Schematic graph represented regions of HBD-TurboID protein. HBD and TurboID
871 were recombined by G_4S linker. NLS and FLAG were recombined in N terminal. B,
872 HBD-TurboID protein expression in 293T stable cell line. C, Estimation of biotinylated
873 whole cell protein by TurboID. D, Sa affinity precipitation (Sa AP) of biotinylated
874 proteins labeled by TurboID system. Sa AP product of biotin linked protein were
875 estimated by PAGE and Sa-HRP. E, Estimation of HBD-TurboID interaction with R-
876 loop associated proteins and reference protein by FLAG IP. F, Estimation of R-loop
877 associated protein by HBD-TurboID system.
878
879 **Figure 2. AKAP8 bind with R-loop and regulated its formation.** A, Estimation of
880 HBD-TurboID interacting with AKAP8 by FLAG IP. B, AKAP8 interacting with R-loop by
881 HBD-TurboID system. C, AKAP8 interacting with R-loop by S9.6 IP. RH: for RNase H
882 treatment. D, F, investigation of AKAP8 interacting with R-loop in A549, HeLa, U2OS,
883 UMSC cells by S9.6 IP. RA: for RNase A treatment. E, immunofluorescence and signal
884 profile of AKAP8, R-loop, rH2A.x in cells. G, Estimation of AKAP8 expressed in shCTRL
885 and shAKAP8. H, I, immunofluorescence and signal profile of AKAP8 and R-loop
886 (S9.6). J, diagram for MYC gene, mRNA and R-loop signal from database and
887 evaluated by DRIP-qPCR. Primer paire 1 2 3 used for promoter, promoter (G4) and
888 exon qPCR analysis.
889
890 **Figure 3. AKAP8 bind with DDX5 in nucleus.** A, GST pull down estimation of
891 AKAP8 interacting with DDX5 in 293T and A549. Input: whole cell extraction. B,
892 AKAP8 interacting with DDX5 by HA IP after benzonase treatment. C, interaction of
893 AKAP8 and DDX5 by IP. D, estimation of GST-AKAP8 and His-DDX5 interaction
894 expressed in E. coli. Input: whole cell extraction of His-DDX5 expression E. coli after
895 IPTG induction.E, immunofluorescence image of AKAP8 and DDX5. F, schematic
896 diagram of structure domain and truncated regions of AKAP8 and DDX5. G,
897 interacting region estimated by truncated HA-AKAP8 and DDX5-FLAG through IP. H,
898 immunofluorescence image of truncated HA-AKAP8 and full length DDX5-FLAG
899 expressed in 293T.
900
901 **Figure 4. AKAP8 knock down increased chromatin DDX5 level.** A, relative
902 transcriptional level of AKAP8 in shCTRL and shAKAP8 293T cell line. B, AKAP8, DDX5
903 expression in shCTRL and shAKAP8 293T cell line. C, Statistic of AKAP8, DDX5
904 expression. D, expression of proteins in cytoplasm (cyto), nucleioplasm (nucleio) and
905 chromatin associated (chromatin) fraction of cell. E, F, Statistic of AKAP8, DDX5
906 expression in cell fractions.
907
908 **Figure 5. RNA-seq revealed AKAP8 regulating pathways.** A, Heat map of
909 clustered DEGs in shCTRL and shAKAP8 cell samples. B, qPCR estimation for relative
910 transcriptional level of selected DEGs. C, statistic for alternative splicing ways for
911 shCTRL and shAKAP8 cell. D, KEGG pathway analysis of up regulated and down
912 regulated DEGs. F, GSEA analysis revealed AKAP8 knock down regulated
913 mitochondrial metabolism pathways.

Figure 6. AKAP8 participated in cell growth and progress of lung carcinoma. A, Z-value estimation of AKAP8 expression across types of cancer. Blue for normal tissue; red for tumor tissue. B, Statistical analysis of AKAP8 expression in lung adenocarcinoma and lung squamous cell carcinoma by comparing that of normal tissue and tumor tissue. C, Survival probability with high and low AKAP8 expression. D, AKAP8 expression level estimation and colony formation for four cells. E, PCA statistics for DEGs set in lung carcinoma tumor and normal tissue.

Figure 7. UCP2 regulated by AKAP8 served as contributing factor to lung adenocarcinoma. A, Survival probability with high and low UCP2 expression. B, Correlation analysis of AKAP8 and UCP2 in LUSC tumor, LUAD tumor and LUAD normal tissue. C, AKAP8 expression in shCTRL and shAKAP8 A549 cell line. D, image of immunofluorescence of AKAP8 and R-loop (S9.6) in shCTRL and shAKAP8 A549 cell lines. E, statistics of relative nuclear signal of AKAP8 and R-loop (S9.6). F, diagram for sketching UCP2 gene, mRNA, DRIP-seq signal. G, relative transcriptional level of UCP2 in shCTRL and shAKAP8 A549 cell lines. H, Estimation of R-loop accumulation in promoter and exon region of UCP2.

Figure S1. AKAP8 bind with R-loop. A, AKAP8 interactome contains RNA process (hnRNPs, Exoscs), chromatin associated (HIST, DPY30) and R-loop associated proteins (RPA, DDX). B, S9.6 IP for estimation of AKAP8 and AKAP8l bind with R-loop. Input: 293T whole cell extraction.

Figure S2. AKAP8 bind with DDX5. A, Co-IP analysis interaction of endogenous expressed AKAP8 and DDX5. B, Co-IP analysis interaction of half-exogenous expressed AKAP8 and DDX5. C, interaction estimation of AKAP8 and DDX5 after benzonase treatment. D, interaction estimation of exogenous AKAP8 and DDX5.

Figure S3. AKAP8 regulated cell metabolism. A, PC analysis of shCTRL and shAKAP8 cell lines. B, Alternative polyadenylation (APA) site motif clustering. C, clustered heatmap of significant TF' in shCTRL and shAKAP8 samples. D, GSEA analysis revealed AKAP8 knock down regulated RNA degradation.

Table S1. Plasmid used in this study.

Table S2. Primers for qPCR used in this study.

Figure 1

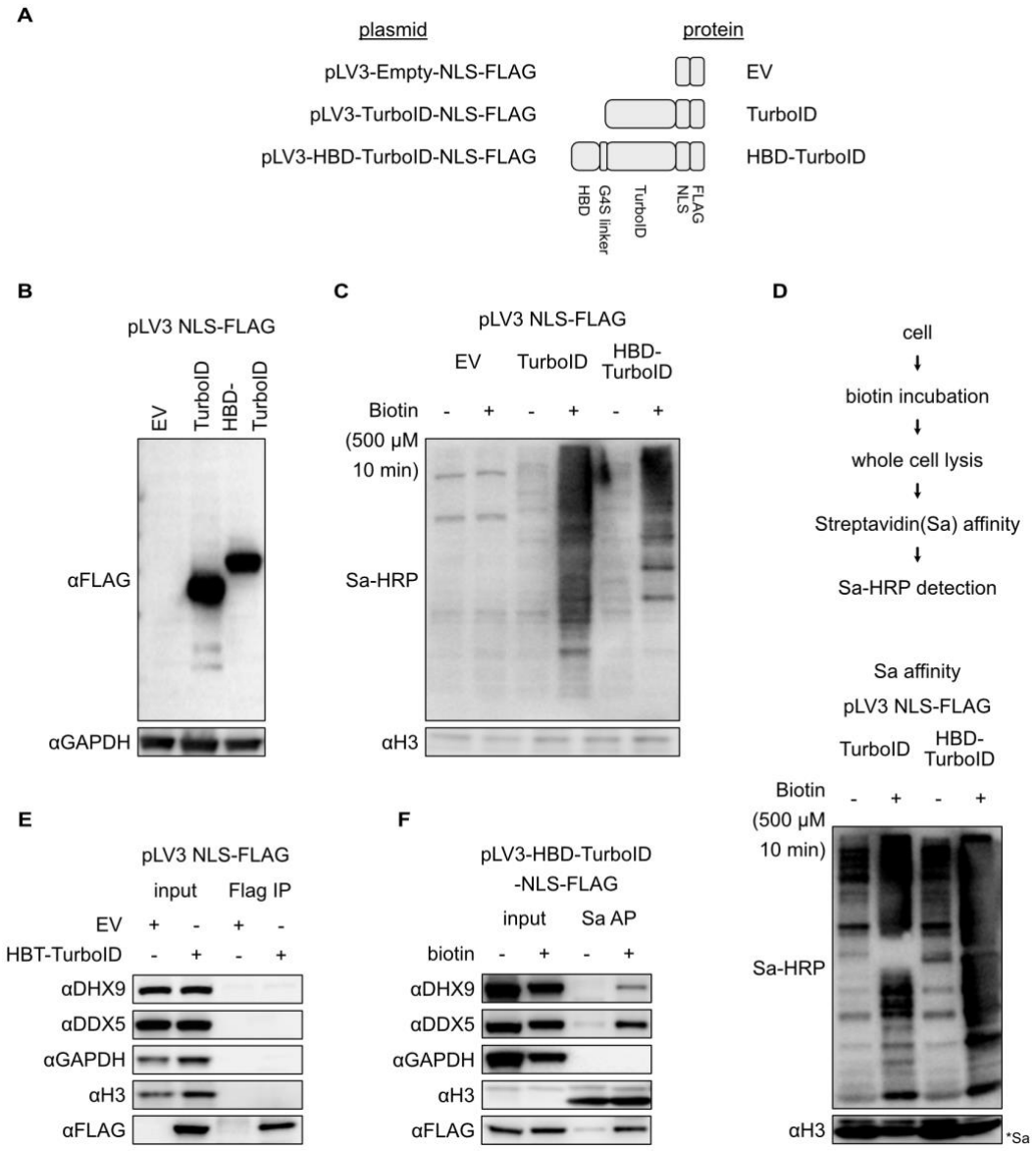
A
plasmid
protein
pLV3-Empty-NLS-FLAG
EV
pLV3-TurboID-NLS-FLAG
TurboID
pLV3-HBD-TurboID-NLS-FLAG
HBD-TurboID
HBD
G4S linker
TurboID
FLAG NLS
B
pLV3 NLS-FLAG
EV
TurboID
HBD-TurboID
αFLAG
αGAPDH
C
pLV3 NLS-FLAG
EV
TurboID
HBD-TurboID
Biotin (500 μM 10 min)
Sa-HRP
αH3
D
cell
biotin incubation
whole cell lysis
Streptavidin(Sa) affinity
Sa-HRP detection
Sa affinity
pLV3 NLS-FLAG
TurboID
HBD-TurboID
Biotin (500 μM 10 min)
Sa-HRP
αH3
*Sa
E
pLV3 NLS-FLAG
input
Flag IP
EV
HBT-TurboID
αDHX9
αDDX5
αGAPDH
αH3
αFLAG
F
pLV3-HBD-TurboID -NLS-FLAG
input
Sa AP
biotin
αDHX9
αDDX5
αGAPDH
αH3
αFLAG

Figure 2

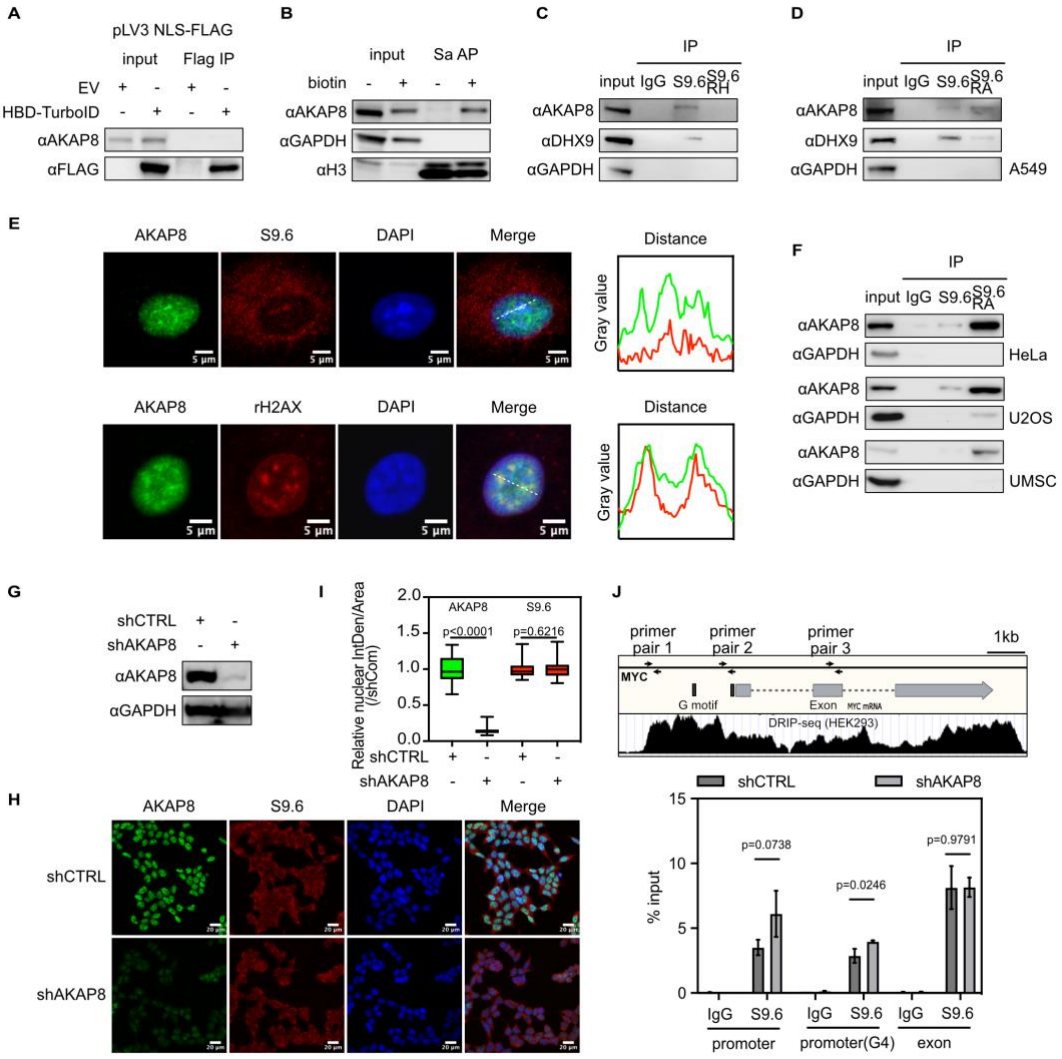
A
pLV3 NLS-FLAG
input
Flag IP
EV
HBD-TurboID
αAKAP8
αFLAG
B
input
Sa AP
biotin
αAKAP8
αGAPDH
αH3
C
IP
input IgG S9.6 S9.6 RH
αAKAP8
αDHX9
αGAPDH
D
IP
input IgG S9.6 S9.6 RA
αAKAP8
αDHX9
αGAPDH
A549
E
AKAP8
S9.6
DAPI
Merge
Distance
Gray value
AKAP8
rH2AX
DAPI
Merge
Distance
Gray value
F
IP
input IgG S9.6 S9.6 RA
αAKAP8
αGAPDH
HeLa
αAKAP8
αGAPDH
U2OS
αAKAP8
αGAPDH
UMSC
G
shCTRL
shAKAP8
αAKAP8
αGAPDH
I
Relative nuclear IntDen/Area (/shCom)
AKAP8
S9.6
p<0.0001
p=0.6216
shCTRL
shAKAP8
H
AKAP8
S9.6
DAPI
Merge
shCTRL
shAKAP8
J
primer pair 1
primer pair 2
primer pair 3
1kb
MYC
G motif
Exon
MYC mRNA
DRIP-seq (HEK293)
shCTRL
shAKAP8
% input
p=0.0738
p=0.0246
p=0.9791
IgG S9.6 IgG S9.6 IgG S9.6
promoter
promoter(G4)
exon

Figure 3

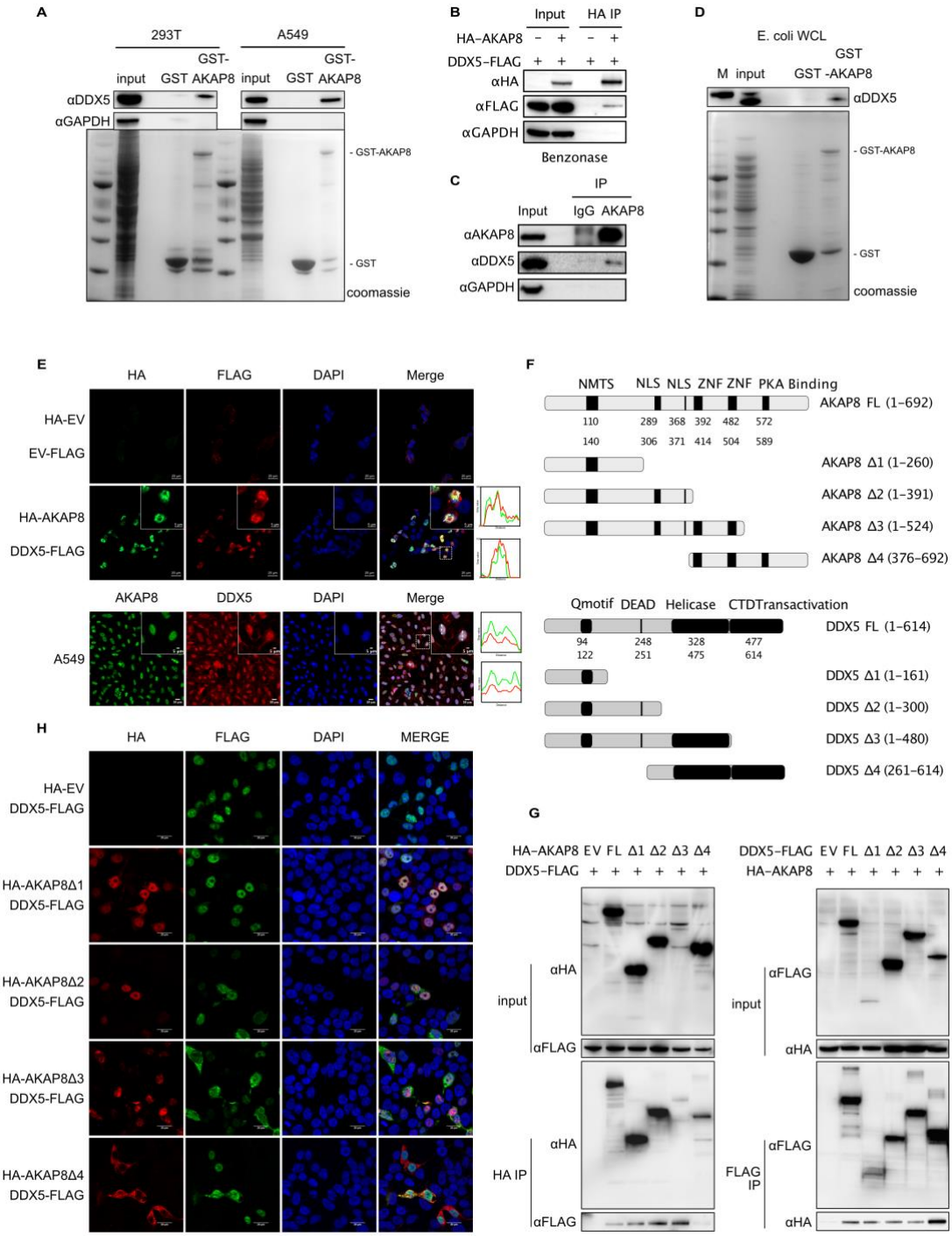
A
293T
A549
input
GST
GST-AKAP8
αDDX5
αGAPDH
- GST-AKAP8
- GST
coomassie
B
Input
HA IP
HA-AKAP8
DDX5-FLAG
αHA
αFLAG
αGAPDH
Benzonase
C
IP
Input
IgG
AKAP8
αAKAP8
αDDX5
αGAPDH
D
E. coli WCL
M
input
GST
GST -AKAP8
αDDX5
- GST-AKAP8
- GST
coomassie
E
HA
FLAG
DAPI
Merge
HA-EV
EV-FLAG
HA-AKAP8
DDX5-FLAG
AKAP8
DDX5
A549
F
NMTS
NLS
ZNF
PKA Binding
AKAP8 FL (1-692)
AKAP8 Δ1 (1-260)
AKAP8 Δ2 (1-391)
AKAP8 Δ3 (1-524)
AKAP8 Δ4 (376-692)
Qmotif
DEAD
Helicase
CTDTransactivation
DDX5 FL (1-614)
DDX5 Δ1 (1-161)
DDX5 Δ2 (1-300)
DDX5 Δ3 (1-480)
DDX5 Δ4 (261-614)
H
MERGE
HA-EV
DDX5-FLAG
HA-AKAP8Δ1
HA-AKAP8Δ2
HA-AKAP8Δ3
HA-AKAP8Δ4
G
HA-AKAP8 EV FL Δ1 Δ2 Δ3 Δ4
DDX5-FLAG
DDX5-FLAG EV FL Δ1 Δ2 Δ3 Δ4
HA-AKAP8
input
αHA
αFLAG
HA IP
FLAG IP

964 Figure 4

965

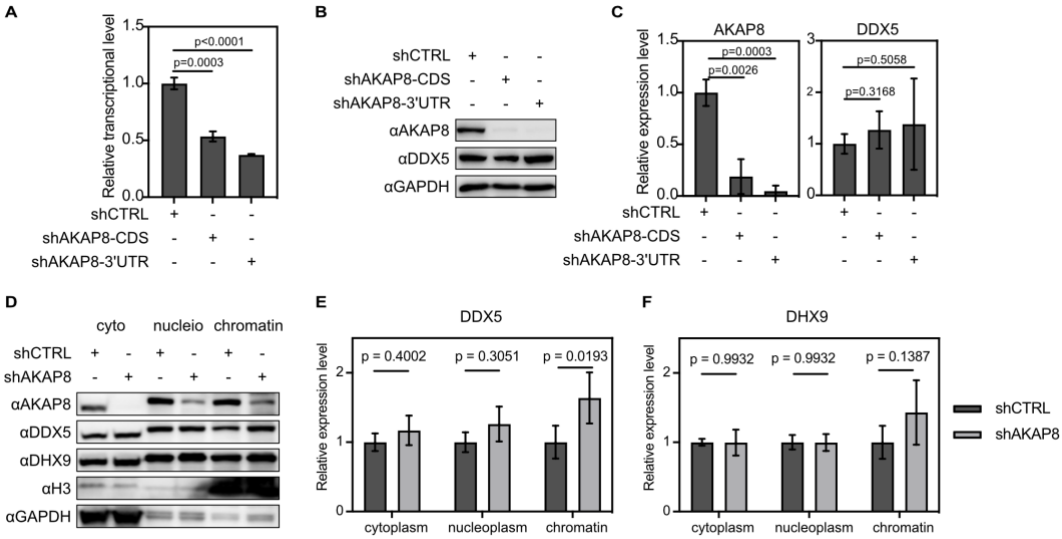

966

967

Figure 5

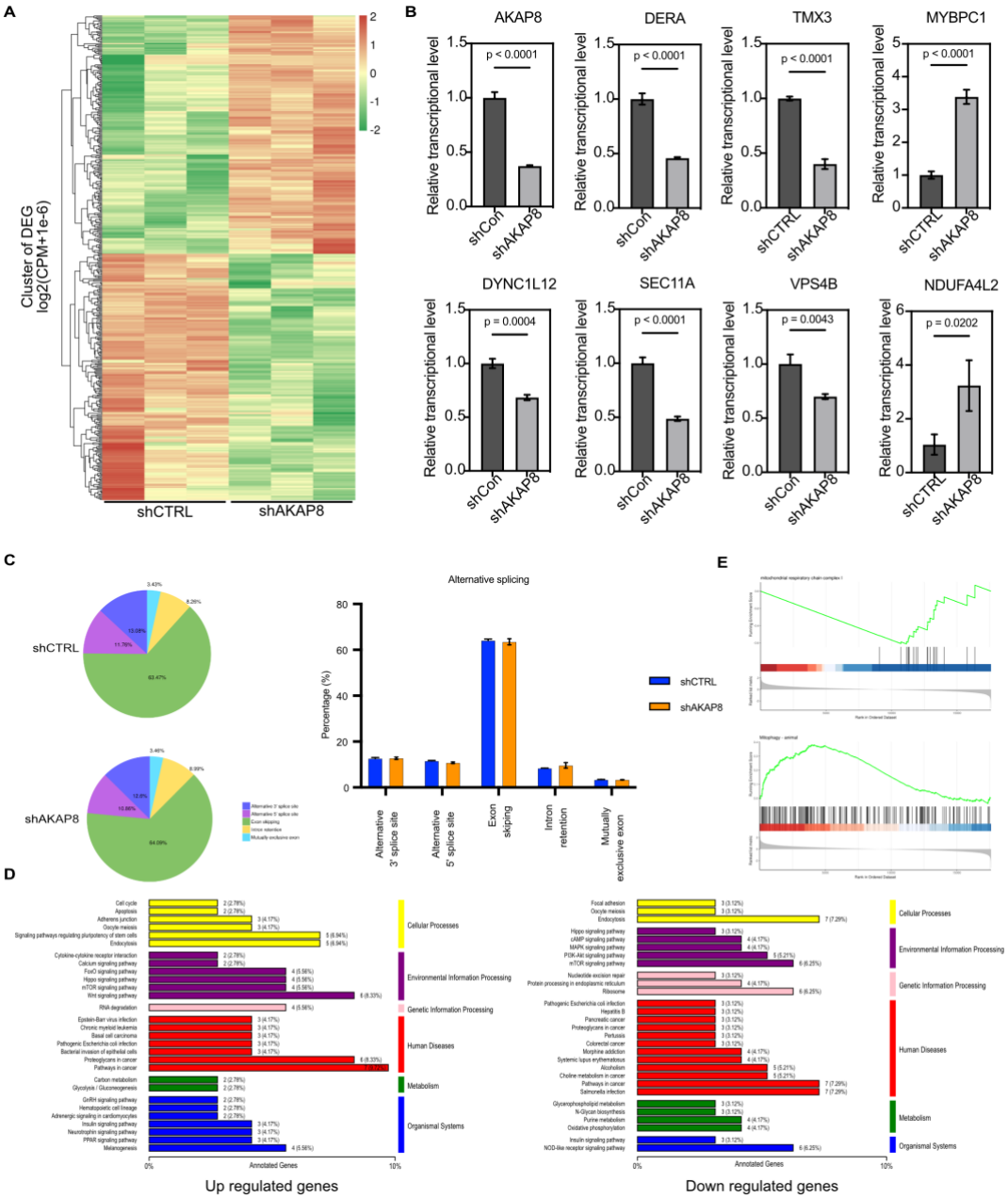
A
Cluster of DEG
log2(CPM+1e-6)
shCTRL
shAKAP8
B
AKAP8
DERA
TMX3
MYBPC1
DYNC1L12
SEC11A
VPS4B
NDUFA4L2
Relative transcriptional level
p < 0.0001
p = 0.0004
p = 0.0043
p = 0.0202
shCon
shAKAP8
shCTRL
C
Alternative splicing
Percentage (%)
Alternative 3' splice site
Alternative 5' splice site
Exon skiping
Intron retention
Mutually exclusive exon
E
D
Cellular Processes
Environmental Information Processing
Genetic Information Processing
Human Diseases
Metabolism
Organismal Systems
Annotated Genes
Up regulated genes
Down regulated genes

Figure 6

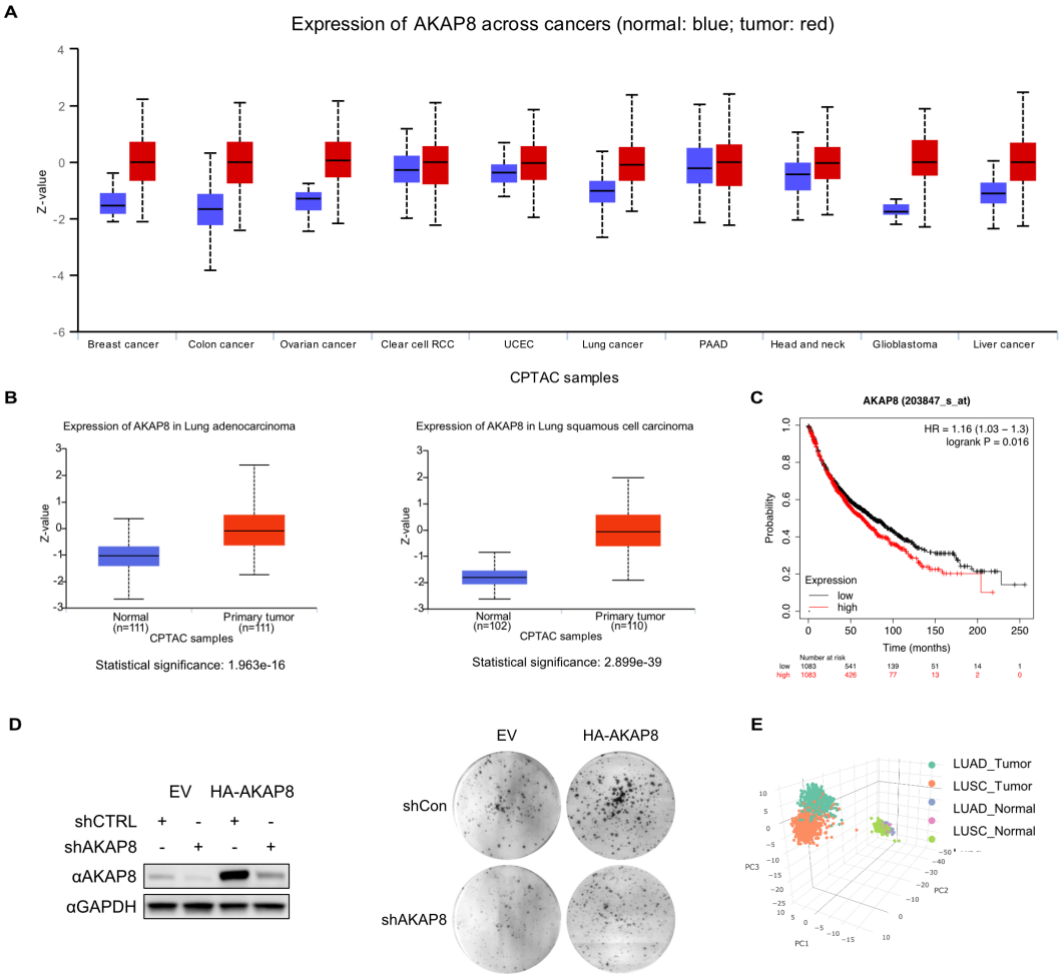
A
Expression of AKAP8 across cancers (normal: blue; tumor: red)
Z-value
Breast cancer
Colon cancer
Ovarian cancer
Clear cell RCC
UCEC
Lung cancer
PAAD
Head and neck
Glioblastoma
Liver cancer
CPTAC samples
B
Expression of AKAP8 in Lung adenocarcinoma
Normal (n=111)
Primary tumor (n=111)
Statistical significance: 1.963e-16
Expression of AKAP8 in Lung squamous cell carcinoma
Normal (n=102)
Primary tumor (n=110)
Statistical significance: 2.899e-39
C
AKAP8 (203847_s_at)
HR = 1.16 (1.03 – 1.3)
logrank P = 0.016
Probability
Expression
low
high
Time (months)
Number at risk
D
EV
HA-AKAP8
shCTRL
shAKAP8
αAKAP8
αGAPDH
shCon
shAKAP8
E
LUAD_Tumor
LUSC_Tumor
LUAD_Normal
LUSC_Normal
PC1
PC2
PC3

Figure 7

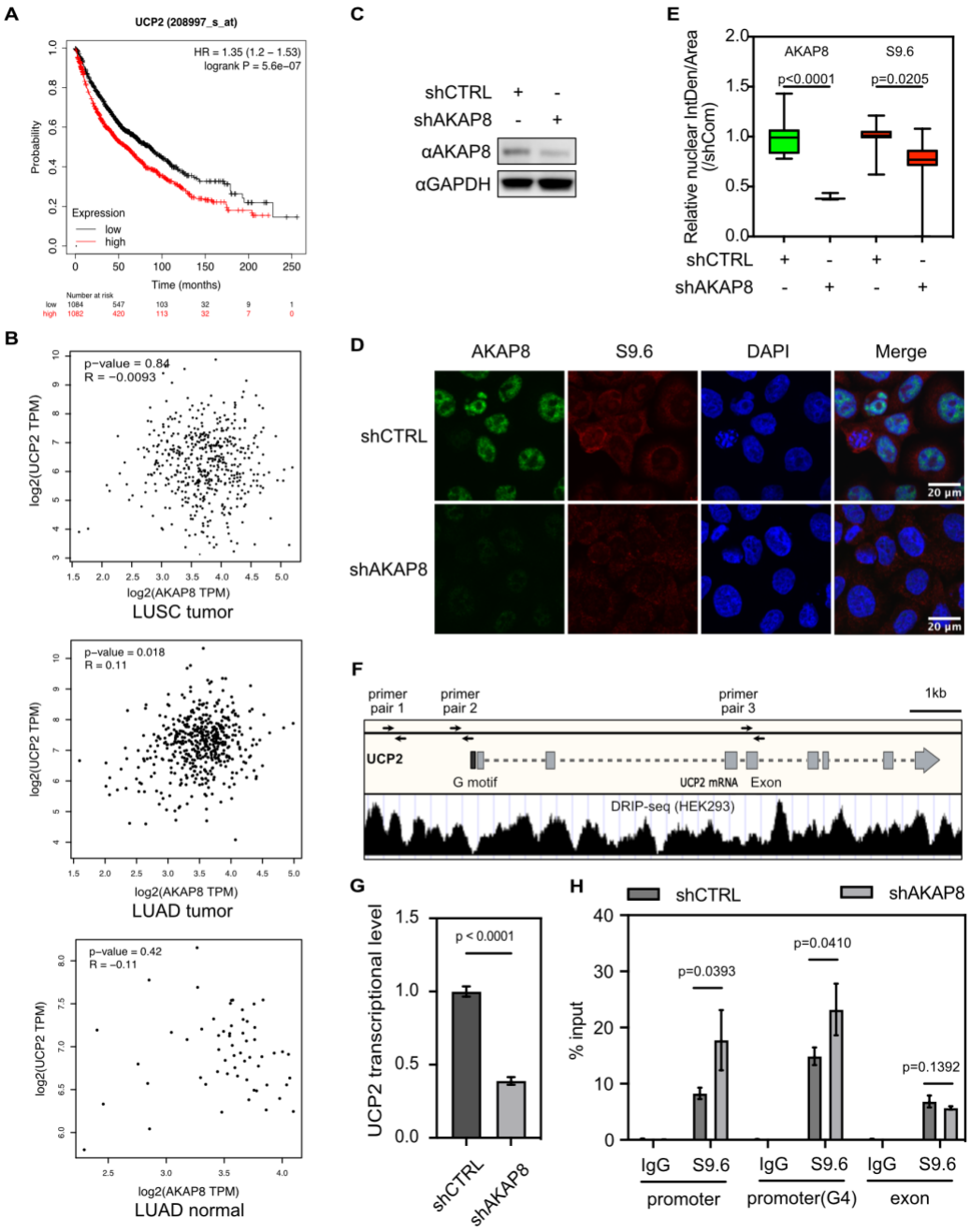
A
UCP2 (208997_s_at)
HR = 1.35 (1.2 – 1.53)
logrank P = 5.6e–07
Probability
Expression
low
high
Time (months)
Number at risk
B
p–value = 0.84
R = –0.0093
log2(UCP2 TPM)
log2(AKAP8 TPM)
LUSC tumor
p–value = 0.018
R = 0.11
LUAD tumor
p–value = 0.42
R = –0.11
LUAD normal
C
shCTRL
shAKAP8
αAKAP8
αGAPDH
D
AKAP8
S9.6
DAPI
Merge
shCTRL
shAKAP8
20 μm
E
Relative nuclear IntDen/Area (/shCom)
AKAP8
S9.6
p<0.0001
p=0.0205
F
primer pair 1
primer pair 2
primer pair 3
1kb
UCP2
G motif
UCP2 mRNA
Exon
DRIP-seq (HEK293)
G
UCP2 transcriptional level
p < 0.0001
shCTRL
shAKAP8
H
shCTRL
shAKAP8
% input
p=0.0393
p=0.0410
p=0.1392
IgG
S9.6
promoter
promoter(G4)
exon